Triaxial rotor model description of $E2$ properties in ^{186,188,190,192}Os

J. M. Allmond,[*] R. Zaballa,[†] A. M. Oros-Peusquens,[‡] W. D. Kulp, and J. L. Wood

School of Physics, Georgia Institute of Technology, Atlanta, Georgia 30332-0430, USA

(Received 4 May 2008; published 2 July 2008)

The triaxial rotor model with independent inertia and electric quadrupole tensors is applied to the description of the extensive set of $E2$ matrix elements available for ^{186,188,190,192}Os. Most large and medium transition $E2$ matrix elements can be reproduced to within $\sim$10%, and most diagonal elements to within $\sim$30%. Most small transition matrix elements can be reproduced to within $\sim$30%, and they support the interference effect exhibited by the model between the inertia and $E2$ tensors: this is a new feature of quantum rotor models. The diagonal $E2$ matrix elements at higher spins in the $K = 2$ band are extremely sensitive to admixtures of higher K values: the low experimental values in ^{190,192}Os indicate significant admixtures of $K = 4$ components. Attention is given to the $K^\pi = 4^+$ bands in these nuclei and the controversial issue of whether they are of quadrupole or hexadecapole nature.

Triaxial rotor models of nuclei have played a leading role in the description of nuclear collectivity ever since their introduction by Davydov in 1958 [1–3]. Triaxial rotations and triaxial shapes are currently at the forefront of modeling phenomenology in odd-mass nuclei and strongly deformed bands (see, e.g., Ref. [4]). However, applications of triaxial rotor models to doubly-even nuclei at low spin has been sparse in the past 20 years [5–8]. With the successes of triaxial descriptions in odd-mass nuclei, it is appropriate to carry out a critical evaluation of such descriptions in doubly even nuclei. In the present work, we do this for the osmium isotopes.

Recently, we introduced [9] a triaxial rotor model with independent inertia and $E2$ tensors. This model overcomes a number of unphysical features [9] possessed by the triaxial rotor model with irrotational moments of inertia, which previously had been the universal choice for the triaxial rotor model. In our initial study [9], we only addressed global features of the model; in the present work, we address the ability of the model to describe detailed $E2$ properties.

The isotopes $^{186-192}$Os constitute a leading challenge to collective models and serve as a best test of models with an axial asymmetry degree of freedom. This is because of their transitional behavior with very low-lying $K^\pi = 2^+$ bands (the 2_2^+ state in ^{192}Os is the *lowest known* 2_2^+ state in any doubly even nucleus) and because there is an extensive set of $E2$ matrix elements available from a multi-Coulomb excitation study [10].

The isotopes ^{190,192}Os also possess a very puzzling feature in their low-lying $K^\pi = 4^+$ bands which exhibit spectro-scopic signatures consistent with multiphonon quadrupole character [10,11], proton two-quasiparticle character [12], and hexadecapole character [13]. This has been the basis of

recent controversy [14–17]. Indeed, this complex character of low-lying $K^\pi = 4^+$ bands may be widely occurring [18]. The triaxial rotor possesses a collective $K^\pi = 4^+$ band, and so we investigate the collective $E2$ properties of these bands in $^{186-192}$Os as triaxial rotor model states.

The triaxial rotor model [9] possesses three energy param-eters A, F, and G ($G < 0$), viz.,

$$\hat{H} = A\hat{I}^2 + F\hat{I}_3^2 + G(\hat{I}_+^2 + \hat{I}_-^2), \quad \hbar = 1; \quad (1)$$

and for $I = 2$,

$$H(2) = \begin{pmatrix} 6A & 4\sqrt{3}G \\ 4\sqrt{3}G & 6A + 4F \end{pmatrix}, \quad (2)$$

$$H(4) = \begin{pmatrix} 20A & 12\sqrt{5}G & 0 \\ 12\sqrt{5}G & 20A + 4F & 4\sqrt{7}G \\ 0 & 4\sqrt{7}G & 20A + 16F \end{pmatrix}. \quad (3)$$

The eigenvectors of $H(2)$ can be expressed as

$$|2_1^+, M\rangle = \cos\Gamma|2, K = 0, M\rangle - \sin\Gamma|2, K = 2, M\rangle,$$

$$|2_2^+, M\rangle = \sin\Gamma|2, K = 0, M\rangle + \cos\Gamma|2, K = 2, M\rangle, \quad (4)$$

where

$$|I, K = 2, M\rangle = \frac{1}{\sqrt{2}}[|I, 2, M\rangle + (-1)^I|I, -2, M\rangle], \quad (5)$$

and

$$\tan 2\Gamma = 2\sqrt{3}\frac{G}{F} \quad (6)$$

(note, $\Gamma < 0$ because $G < 0$). (We drop the M quantum number from here on.)

Further, the model [9] possesses two parameters, Q_0 and γ, describing the $E2$ properties (in units of eb)

$$\hat{T}(E2) = \sqrt{\frac{5}{16\pi}}\left[\cos\gamma\,\hat{T}_0^{(2)} + \frac{\sin\gamma}{\sqrt{2}}\left(\hat{T}_{+2}^{(2)} + \hat{T}_{-2}^{(2)}\right)\right], \quad (7)$$

where the $\hat{T}_\nu^{(2)}$ reduce to

$$\langle I_f K_f \| \hat{T}_{\pm\nu}^{(2)} \| I_i K_i \rangle = Q_0\sqrt{2I_i + 1}\langle I_i K_i; 2, \pm\nu | I_f K_f \rangle. \quad (8)$$

---

*Current address: Department of Physics, University of Richmond, VA 23173, USA.

†Current address: Department of Physics and Astronomy, Georgia State University, Atlanta, GA 30303, USA.

‡Current address: Institute of Medicine, MR Group, Research Centre Juelich, D-52425 Juelich, Germany.
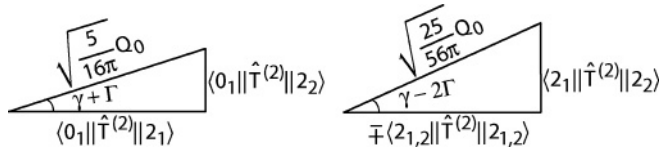
FIG. 1. Representation of model parameters in the $I = 0, 2$ subspace. This is useful for correlating the reduced $E2$ matrix element strengths and shape asymmetries. Since $\langle 0_1 \| \hat{T}(E2) \| 2_1 \rangle$ is usually the most precisely known reduced $E2$ matrix element and since it is controlled by the smallest angle (Γ is negative), Q_0 is generally extracted from the left triangle relation.

The parameters A and F are directly determined from the experimental energies $E(2_1^+)$ and $E(2_2^+)$ because $|G| \ll F$. The parameters G, γ, and Q_0 are determined via the $E2$ matrix elements[1]

$$\langle 0_1 \| \hat{T}(E2) \| 2_1 \rangle = \sqrt{\frac{5}{16\pi}} Q_0 \cos(\gamma + \Gamma), \quad (9)$$

$$\langle 0_1 \| \hat{T}(E2) \| 2_2 \rangle = \sqrt{\frac{5}{16\pi}} Q_0 \sin(\gamma + \Gamma), \quad (10)$$

$$\langle 2_1 \| \hat{T}(E2) \| 2_2 \rangle = \sqrt{\frac{25}{56\pi}} Q_0 \sin(\gamma - 2\Gamma), \quad (11)$$

$$\langle 2_1 \| \hat{T}(E2) \| 2_1 \rangle = -\sqrt{\frac{25}{56\pi}} Q_0 \cos(\gamma - 2\Gamma)$$
$$= -\langle 2_2 \| \hat{T}(E2) \| 2_2 \rangle, \quad (12)$$

using Eqs. (9)–(11) or Eqs. (10)–(12). Equations (9)–(12) are usefully depicted as shown in Fig. 1.

The parameters Q_0 and γ can alternatively be determined using the corresponding $B(E2)$'s,

$$B(E2; I_i \to I_f) = \frac{\langle I_f \| \hat{T}(E2) \| I_i \rangle^2}{(2I_i + 1)}, \quad (13)$$

and quadrupole moments,

$$Q(2_1^+) = -\frac{2}{7} Q_0 \cos(\gamma - 2\Gamma) = -Q(2_2^+). \quad (14)$$

We apply the model [9] to the extensive set of $E2$ matrix elements reported by Wu *et al.* [10]. These matrix elements are given in Table I. The experimental level energies for $^{186-192}$Os are shown in Fig. 2. Using the above formalism, the model parameters for ^{186}Os are

$$A = \frac{1}{6} E(2_1^+) = 22.86 \, \text{keV}, \quad (15)$$

$$F = \frac{1}{4}[E(2_2^+) - E(2_1^+)] = 157.6 \, \text{keV}, \quad (16)$$

$$Q_0 = \sqrt{\frac{16\pi}{5}} \sqrt{\langle 0_1 \| \hat{T}(E2) \| 2_1 \rangle^2 + \langle 0_1 \| \hat{T}(E2) \| 2_2 \rangle^2}$$
$$= 5.582 \, e\text{b}, \quad (17)$$

$$\gamma + \Gamma = \tan^{-1}\left(\frac{\langle 0_1 \| \hat{T}(E2) \| 2_2 \rangle}{\langle 0_1 \| \hat{T}(E2) \| 2_1 \rangle}\right), \quad (18)$$

---

[1] We note here that a factor of $\sqrt{5}$ was inadvertently omitted from the right-hand sides of Eqs. (17)–(21) in Ref. [9].

TABLE I. Experimental [10] $E2$ matrix elements, $\langle I_f \| \hat{T}(E2) \| I_i \rangle$'s ($e$b), for $^{186-192}$Os.

	^{186}Os	^{188}Os	^{190}Os	^{192}Os
$2_1 - 0_1$	1.674^{+25}_{-21}	1.585^{+10}_{-10}	1.530^{+20}_{-11}	1.456^{+8}_{-9}
$4_1 - 2_1$	2.761^{+61}_{-70}	2.642^{+25}_{-20}	2.367^{+80}_{-31}	2.115^{+29}_{-28}
$6_1 - 4_1$	3.89^{+8}_{-5}	3.31^{+4}_{-4}	2.970^{+63}_{-40}	2.930^{+74}_{-44}
$8_1 - 6_1$	4.32^{+11}_{-10}	3.97^{+11}_{-11}	3.72^{+10}_{-10}	3.58^{+10}_{-9}
$10_1 - 8_1$	5.02^{+93}_{-60}	5.00^{+34}_{-21}	3.98^{+44}_{-39}	3.80^{+16}_{-48}
$12_1 - 10_1$	5.16^{+38}_{-131}	3.76^{+30}_{-30}	$\oslash$	$\oslash$
$4_2 - 2_2$	1.965^{+87}_{-66}	1.78^{+7}_{-5}	1.871^{+42}_{-37}	1.637^{+24}_{-33}
$6_2 - 4_2$	2.78^{+18}_{-11}	2.46^{+10}_{-10}	2.60^{+12}_{-13}	2.09^{+6}_{-13}
$8_2 - 6_2$	3.26^{+35}_{-28}	2.55^{+22}_{-69}	2.60^{+36}_{-19}	2.31^{+17}_{-16}
$10_2 - 8_2$	3.45^{+88}_{-40}	$\oslash$	$\oslash$	$\oslash$
$2_2 - 0_1$	0.545^{+13}_{-7}	0.483^{+2}_{-9}	0.444^{+9}_{-7}	0.430^{+8}_{-4}
$2_2 - 2_1$	0.897^{+64}_{-14}	0.865^{+11}_{-11}	1.065^{+20}_{-37}	1.230^{+34}_{-16}
$4_1 - 2_2$[a]	0.227^{+32}_{-32}	0.378^{+50}_{-63}	0.19^{+12}_{-9}	0.35^{+16}_{-4}
$4_2 - 2_1$	0.419^{+27}_{-15}	0.283^{+8}_{-8}	0.203^{+7}_{-7}	0.130^{+5}_{-8}
$4_2 - 4_1$	1.220^{+62}_{-55}	1.10^{+3}_{-3}	1.435^{+43}_{-45}	1.35^{+8}_{-4}
$6_1 - 4_2$[a]	0.67^{+30}_{-12}	0.57^{+7}_{-12}	0.66^{+26}_{-8}	0.40^{+9}_{-9}
$6_2 - 4_1$	$\pm 0.325^{+20}_{-26}$	$\pm 0.127^{+6}_{-12}$	0.195^{+75}_{-74}	$\pm 0.069^{+157}_{-73}$
$6_2 - 6_1$	1.37^{+9}_{-11}	1.46^{+13}_{-25}	1.76^{+20}_{-15}	1.49^{+15}_{-6}
$2_1 - 2_1$	-1.75^{+22}_{-13}	-1.73^{+19}_{-5}	-1.25^{+22}_{-13}	-1.21^{+6}_{-17}
$4_1 - 4_1$	-2.02^{+39}_{-18}	-2.00^{+9}_{-20}	-1.28^{+27}_{-19}	-0.73^{+26}_{-6}
$6_1 - 6_1$	-1.67^{+29}_{-31}	-1.60^{+18}_{-33}	-0.91^{+24}_{-15}	-1.16^{+11}_{-26}
$8_1 - 8_1$	-2.26^{+24}_{-108}	-1.38^{+44}_{-26}	-0.94^{+49}_{-41}	-1.31^{+18}_{-36}
$2_2 - 2_2$	2.12^{+6}_{-22}	2.10^{+9}_{-6}	1.53^{+6}_{-31}	0.985^{+45}_{-85}
$4_2 - 4_2$	-1.12^{+25}_{-23}	-1.22^{+16}_{-10}	-1.29^{+20}_{-25}	-0.83^{+9}_{-8}
$6_2 - 6_2$	$\oslash$	-1.33^{+23}_{-56}	-0.80^{+47}_{-27}	-1.35^{+11}_{-37}
$8_2 - 8_2$	$\oslash$	$\oslash$	-1.05^{+62}_{-38}	-0.91^{+49}_{-34}
$4_3 - 2_1$	0.08^{+5}_{-8}	0.123^{+23}_{-23}	0.052^{+5}_{-7}	0.115^{+45}_{-31}
$4_3 - 2_2$	1.19^{+13}_{-14}	0.83^{+4}_{-3}	0.77^{+5}_{-5}	0.786^{+37}_{-37}
$4_3 - 3_1$[a]	-1.52^{+9}_{-29}	-1.17^{+17}_{-5}	-1.55^{+7}_{-40}	-1.63^{+11}_{-22}
$4_3 - 4_2$	1.83^{+32}_{-34}	1.64^{+7}_{-7}	1.59^{+11}_{-17}	1.19^{+8}_{-7}
$4_3 - 4_3$	2.35^{+92}_{-69}	2.68^{+22}_{-19}	1.02^{+18}_{-4}	1.28^{+15}_{-41}

[a] For an even-rank operator, $\langle I_f \| \hat{T}(E2) \| I_i \rangle = (-1)^{I_i + I_f} \langle I_i \| \hat{T}(E2) \| I_f \rangle$.

$$\gamma - 2\Gamma = \sin^{-1}\left(\sqrt{\frac{56\pi}{25}} \frac{\langle 2_1 \| \hat{T}(E2) \| 2_2 \rangle}{Q_0}\right), \quad (19)$$
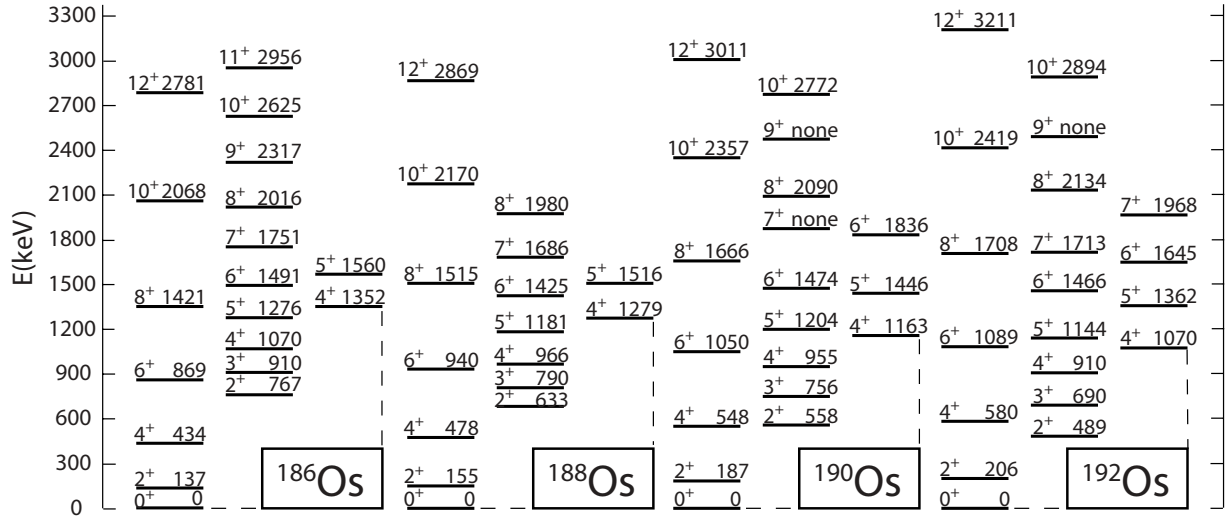
whence

$$\Gamma = -0.0419 \, \text{rad} \, (-2.40°), \quad (20)$$
$$\gamma = 0.3566 \, \text{rad} \, (20.43°), \quad (21)$$

and

$$G = \frac{F}{2\sqrt{3}} \tan(2\Gamma) = -3.82 \, \text{keV}. \quad (22)$$

Equation (12) yields $\langle 2_1 \| \hat{T}(E2) \| 2_1 \rangle = -\langle 2_2 \| \hat{T}(E2) \| 2_2 \rangle = -1.90 \, e$b, which can be compared with the experimental

FIG. 2. Energy levels for $^{186-192}$Os showing the lowest $K = 0$, 2, and 4 bands. The data are from the Nuclear Data Sheets [19–22].

values of $\langle 2_1 \| \hat{T}(E2) \| 2_1 \rangle = -1.75^{+22}_{-13}$ eb and $\langle 2_2 \| \hat{T}(E2) \| 2_2 \rangle = 2.12^{+6}_{-22}$ eb. Table II shows the choices for the parameters for all four Os isotopes under study.

We note that there are other $E2$ data available for the osmium isotopes. The recent lifetime measurements in ^{188,190}Os (up to spin 8^+ in the ground band, up to spin 6^+ in the γ band, and for the 4^+ state of the $K^\pi = 4^+$ band) by Wu et al. [11] yield $B(E2)$ values that agree with $B(E2)$ values calculated using the $E2$ matrix elements in Table I. Coulomb excitation studies carried out prior to the work of Wu et al. [10] are more limited in scope and generally less precise and so were not considered for the present study. A muonic x-ray study by Hoehn et al. [23] reports values for $B(E2; 0^+_1 \rightarrow 2^+_1)$ and $Q(2^+_1)$ for $^{186-192}$Os. The $B(E2)$ values show fair to good consistency with the corresponding $E2$ matrix elements. The $Q(2^+_1)$ values show only moderate consistency with the corresponding $E2$ matrix elements. Details are given later.

Equation (3) and the values of F and G in Table I immediately suggest a useful approximation in applying the model: for properties of the $K = 0$ and $K = 2$ bands, the influence of higher K bands appears likely to be negligible, because $4\sqrt{7}|G| \ll [E(K = 4) - E(K = 2)] = 12F$. Thus, we first study a two-state mixing description within the triaxial rotor model, for which

$$H(I) = \begin{pmatrix} AI(I+1) & G\sqrt{2(I-1)I(I+1)(I+2)} \\ G\sqrt{2(I-1)I(I+1)(I+2)} & AI(I+1) + 4F \end{pmatrix}, \tag{23}$$

$I = 2, 4, 6, 8, \ldots$ (the $I = 3, 5, 7, \ldots$ states in the $K = 2$ band will be unmixed). The resulting mixing angles for the even-spin states are given by

$$\tan(2\Gamma_I) = \sqrt{\frac{(I-1)I(I+1)(I+2)}{24}} \tan(2\Gamma). \tag{24}$$

TABLE II. Parameter values for $^{186-192}$Os. Note that G depends on Γ, cf. Eq. (6).

Mass	A (keV)	F (keV)	Q_0 (eb)	γ (deg)	Γ (deg)	G (keV)
186	22.86	157.6	5.582	20.43	−2.40	−3.82
188	25.84	119.5	5.254	19.93	−2.98	−3.60
190	31.12	92.8	5.051	22.12	−5.94	−5.64
192	34.30	70.8	4.814	25.19	−8.74	−6.44

Following reduction using the Wigner-Eckart theorem, the $E2$ matrix elements involving $I > 2$ do not have the simple forms manifested in Eqs. (9)–(12), except

$$\langle 2_1 \| \hat{T}(E2) \| 3_1 \rangle = \sqrt{\frac{25}{32\pi}} Q_0 \sin(\gamma + \Gamma), \tag{25}$$

$$\langle 2_2 \| \hat{T}(E2) \| 3_1 \rangle = -\sqrt{\frac{25}{32\pi}} Q_0 \cos(\gamma + \Gamma), \tag{26}$$

$$\langle 3_1 \| \hat{T}(E2) \| 3_1 \rangle = 0, \tag{27}$$

and for I odd

$$\langle I_f \| \hat{T}(E2) \| I_i \rangle = Q_0 \sqrt{\frac{5}{16\pi}} \sqrt{2I_i + 1} \cos\gamma \langle I_i 2; 20 | I_f 2 \rangle, \tag{28}$$

TABLE III. Values of $\langle\|E2\|\rangle eb$ calculated using $K = 0, 2$ (two-band) mixing as described in the text for $^{186-192}$Os. The % values are the differences $(\langle\|E2\|\rangle_{\text{th}} - \langle\|E2\|\rangle_{\text{ex}}) \times 100/|\langle\|E2\|\rangle_{\text{ex}}|$. The values are given to one decimal place more than the experimental quantities. The values of Q_0, γ, and Γ, which are all that are needed for $E2$ properties, are taken from Table II.

	^{186}Os	^{188}Os	^{190}Os	^{192}Os
$2_1 - 0_1$	$1.6741^{(\text{fit})}$	$1.5851^{(\text{fit})}$	$1.5299^{(\text{fit})}$	$1.4561^{(\text{fit})}$
$4_1 - 2_1$	$2.7281 \, (-1.2\%)$	$2.5840 \, (-2.2\%)$	$2.4933 \, (+5.3\%)$	$2.3673 \, (+11.9\%)$
$6_1 - 4_1$	$3.533 \, (-9.2\%)$	$3.351 \, (+1.2\%)$	$3.2769 \, (+10.3\%)$	$3.1438 \, (+7.3\%)$
$8_1 - 6_1$	$4.257 \, (-1.5\%)$	$4.039 \, (+1.7\%)$	$3.946 \, (+6.1\%)$	$3.770 \, (+5.3\%)$
$10_1 - 8_1$	$4.903 \, (-2.3\%)$	$4.640 \, (-7.5\%)$	$4.501 \, (+13.1\%)$	$4.290 \, (+12.9\%)$
$12_1 - 10_1$	$5.466 \, (+5.9\%)$	$5.160 \, (+31.4\%)$	$4.985 \, (\oslash)$	$4.748 \, (\oslash)$
$4_2 - 2_2$	$1.6505 \, (-16.0\%)$	$1.547 \, (-13.1\%)$	$1.3996 \, (-25.2\%)$	$1.2488 \, (-23.7\%)$
$6_2 - 4_2$	$2.674 \, (-3.8\%)$	$2.498 \, (+1.5\%)$	$2.259 \, (-13.1\%)$	$2.032 \, (-2.8\%)$
$8_2 - 6_2$	$3.244 \, (-0.5\%)$	$3.043 \, (+19.3\%)$	$2.784 \, (+7.1\%)$	$2.506 \, (+8.5\%)$
$10_2 - 8_2$	$3.682 \, (+6.7\%)$	$3.470 \, (\oslash)$	$3.195 \, (\oslash)$	$2.877 \, (\oslash)$
$2_2 - 0_1$	$0.5449^{(\text{fit})}$	$0.4831^{(\text{fit})}$	$0.4439^{(\text{fit})}$	$0.4299^{(\text{fit})}$
$2_2 - 2_1$	$0.8969^{(\text{fit})}$	$0.8648^{(\text{fit})}$	$1.0647^{(\text{fit})}$	$1.2300^{(\text{fit})}$
$2_2 - 4_1$	$0.3156 \, (+39.0\%)$	$0.3222 \, (-14.8\%)$	$0.407 \, (+114.4\%)$	$0.409 \, (+17.0\%)$
$4_2 - 2_1$	$0.2834 \, (-32.4\%)$	$0.1776 \, (-37.2\%)$	$-0.0638 \, (-131.4\%)$	$-0.1498 \, (-215.2\%)$
$4_2 - 4_1$	$1.2722 \, (+4.3\%)$	$1.198 \, (+8.9\%)$	$1.2537 \, (-12.6\%)$	$1.215 \, (-10.0\%)$
$4_2 - 6_1$	$0.630 \, (-6.0\%)$	$0.604 \, (+6.0\%)$	$0.498 \, (-24.5\%)$	$0.328 \, (-17.9\%)$
$6_2 - 4_1$	$0.0747 \, (-77.0\%)$	$-0.0340 \, (-126.8\%)$	$-0.1690 \, (-186.7\%)$	$-0.1208 \, (-275.1\%)$
$6_2 - 6_1$	$1.340 \, (-2.2\%)$	$1.191 \, (-18.4\%)$	$0.978 \, (-44.4\%)$	$0.832 \, (-44.1\%)$
$2_1 - 2_1$	$-1.903 \, (-8.8\%)$	$-1.782 \, (-3.0\%)$	$-1.579 \, (-26.3\%)$	$-1.334 \, (-10.3\%)$
$4_1 - 4_1$	$-2.148 \, (-6.3\%)$	$-1.954 \, (+2.3\%)$	$-1.431 \, (-11.8\%)$	$-0.982 \, (-34.6\%)$
$6_1 - 6_1$	$-2.155 \, (-29.0\%)$	$-1.926 \, (-20.4\%)$	$-1.357 \, (-49.1\%)$	$-0.955 \, (+17.6\%)$
$8_1 - 8_1$	$-2.127 \, (+5.9\%)$	$-1.928 \, (-39.7\%)$	$-1.457 \, (-54.9\%)$	$-1.081 \, (+17.48\%)$
$2_2 - 2_2$	$1.903 \, (-10.2\%)$	$1.782 \, (-15.2\%)$	$1.579 \, (+3.2\%)$	$1.3343 \, (+35.5\%)$
$4_2 - 4_2$	$-1.384 \, (-23.5\%)$	$-1.381 \, (-13.2\%)$	$-1.728 \, (-33.9\%)$	$-1.959 \, (-136.0\%)$
$6_2 - 6_2$	$-2.990 \, (\oslash)$	$-2.932 \, (-120.5\%)$	$-3.246 \, (-305.7\%)$	$-3.329 \, (-146.6\%)$
$8_2 - 8_2$	$-4.141 \, (\oslash)$	$-3.990 \, (\oslash)$	$-4.151 \, (-295.3\%)$	$-4.139 \, (-354.8\%)$

where $\langle I_i 2; 20|I_f 2\rangle$ is a Clebsch-Gordan coefficient. The $E2$ matrix elements are given here in general form for 2×2 mixing in the g-band ($K = 0$) and γ-band ($K = 2$) subspace,[2]

$$|I2\rangle_\diamond \equiv \frac{1}{\sqrt{2}}\left(|I2\rangle + (-1)^{I+2}|I, -2\rangle\right), \quad (29)$$

$$|I0\rangle_\diamond \equiv |I0\rangle, \quad (30)$$

$$|I_i\rangle = c_1|I_i 0\rangle_\diamond + c_2|I_i 2\rangle_\diamond, \quad (31)$$

$$|I_f\rangle = c_3|I_f 0\rangle_\diamond + c_4|I_f 2\rangle_\diamond, \quad (32)$$

$$\begin{aligned}
\langle I_f\|\hat{T}(E2)\|I_i\rangle = {} & Q_0\sqrt{\frac{5}{16\pi}}\sqrt{2I_i + 1} \\
& \times \{c_1 c_3 \cos\gamma \, \langle I_i 0; 20|I_f 0\rangle \\
& + c_1 c_4 \sin\gamma \, \langle I_i 2; 2, -2|I_f 0\rangle \\
& + c_2 c_3 \sin\gamma \, \langle I_i 0; 22|I_f 2\rangle \\
& + c_2 c_4 \cos\gamma \, \langle I_i 2; 20|I_f 2\rangle\},
\end{aligned} \quad (33)$$

These general matrix elements apply to odd spin as well (e.g., $c_1 = c_3 = 0$ and $c_2 = c_4 = 1$). For even spin, the c's are the amplitudes $\cos\Gamma_I$ and $\sin\Gamma_I$.

The results of our two-band mixing calculations, using the parameters given in Table II, are shown in Table III. The fits can be summarized: (excluding the three matrix elements used to determine Q_0, γ, and Γ in each nucleus) 26 out of 31 intraband transition matrix elements are fitted to better than 14%; 17 out of 24 interband transition matrix elements are fitted to better than 45%; 20 of the 29 diagonal matrix elements are fitted to better than 35%. There are notable failures for $\Delta I = -2$ interband transitions and $K = 2$ band diagonal matrix elements. We explore these failures below.

The reliability of the values of Q_0 in each of the Os isotopes, cf. Table II and Eq. (17), is reflected in the agreement for the ground-band (both off-diagonal and diagonal) and γ-band

---

[2]We use γ to designate the triaxiality angle of the electric quadrupole tensor and, separately, the $K = 2$ band in the model space.

TABLE IV. Comparison of the present triaxial calculations to Hoehn *et al.*'s muonic x-ray data [23].

	Triaxial calc (eb)[a]	Hoehn exp (eb) [23]	% diff
^{186}Os			
$\langle 2_1 \| \hat{T}(E2) \| 0_1 \rangle$	1.6741	1.775[8]	−5.7%
$\langle 2_1 \| \hat{T}(E2) \| 2_1 \rangle$	−1.903	−2.15[6]	11.5%
^{188}Os			
$\langle 2_1 \| \hat{T}(E2) \| 0_1 \rangle$	1.5851	1.679[9]	−5.6%
$\langle 2_1 \| \hat{T}(E2) \| 2_1 \rangle$	−1.782	−1.93[5]	7.7%
^{190}Os			
$\langle 2_1 \| \hat{T}(E2) \| 0_1 \rangle$	1.5299	1.568[7]	−2.4%
$\langle 2_1 \| \hat{T}(E2) \| 2_1 \rangle$	−1.579	−1.56[4]	−1.2%
^{192}Os			
$\langle 2_1 \| \hat{T}(E2) \| 0_1 \rangle$	1.4561	1.449[7]	0.5%
$\langle 2_1 \| \hat{T}(E2) \| 2_1 \rangle$	−1.334	−1.27[4]	−5.0%

[a]$\langle 2_1 \| \hat{T}(E2) \| 0_1 \rangle$ was fitted to Wu *et al.*'s Coulex data [10], and $\langle 2_1 \| \hat{T}(E2) \| 2_1 \rangle$ was predicted by the theory from that fit.

(off-diagonal) $E2$ matrix elements shown in Table III. We note that among these matrix elements, the largest deviation is for ^{190}Os $8_1 - 8_1 (-54.9\%)$ and the experimental uncertainty is $+52\%/-44\%$. The $\langle 2_1 \| \hat{T}(E2) \| 0_1 \rangle$ and $\langle 2_1 \| \hat{T}(E2) \| 2_1 \rangle$ matrix elements deduced from the muonic x-ray study by Hoehn *et al.* are compared with our calculations in Table IV.

Ascertaining the reliability of the values of γ and Γ is a very challenging task for two reasons. First, these two parameters act to destructively interfere for certain matrix elements, cf. Eq. (10) for $0_1 - 2_2$, where it should be noted that γ and Γ have opposite signs and this matrix element involves the sine of an angle less than $20°$ and so changes rapidly with angle. Second, the experimental uncertainties, cf. Table I, range from about $\sim 1\%$ to $\sim 50\%$ and are asymmetrical. Therefore, we employed "error band" plots, as shown in Figs. 3–6, to determine the sensitivity of γ and Γ to the experimental data. The discussion of this follows.

Figures 3 and 4 show the variation in the model $E2$ matrix elements for ^{186,192}Os as a function of γ. The plots are separated into diagonal, intraband off-diagonal, and interband matrix elements. This separation reveals the orders-of-magnitude difference in their sensitivity to γ and is directly understood in terms of their sine and cosine dependence, Eqs. (9)–(12); i.e., for $\gamma \sim 20°$, $\Gamma \sim -5°$: diagonal $\sim \cos 30°$, intraband off-diagonal $\sim \cos 15°$, interband ($\Delta I = 0$) $\sim \sin 30°$, and interband ($\Delta I = -2$) $\sim \sin 15°$ (the prefactors are all about $0.35 Q_0$).

The extreme sensitivity of the $\Delta I = -2$, $\Delta K = -2$ $E2$ matrix elements to Γ_I reveals that the model relationship, Eq. (24), breaks down. This is illustrated in Fig. 7 which shows that to fit these matrix elements exactly, Γ must decrease with increasing spin.

The most serious failures are for diagonal matrix elements. This appears to be more severe for the γ band than the ground band and to be somewhat more severe in the heavier Os isotopes. This feature of the model comparison appears to be contradictory because the transition matrix elements in the ground band and γ band are uniformly well described (e.g., in ^{190}Os, $8_2 - 6_2$ is reproduced to within 7.1%, whereas $8_2 - 8_2$ deviates by 295% and $6_2 - 6_2$ deviates by 306%); however, we explain this later. Other features of note are itemized below.

The deviations of the γ-band transition matrix elements all vary monotonically from the model values, being less than experiment at low spin and greater than experiment at high spin. This feature is counter intuitive because any variation is expected to be toward larger $E2$ strengths at higher spin as a result of centrifugal stretching. Furthermore, no parallel effect is observed for the ground-band transition matrix elements. We present an explanation later.

The fitted values of γ and Q_0 show, cf. Fig. 8(a), a reciprocal correlation. Indeed, the quantity $Q_0 \sin \gamma$ is remarkably constant, viz., 1.95 (^{186}Os), 1.79 (^{188}Os), 1.90 (^{190}Os), and 2.05 eb (^{192}Os). This is an effect that has been noted [24] to occur widely in fits of the Davydov-Filippov model [1], i.e., using irrotational moments of inertia. The fitted values of Γ are
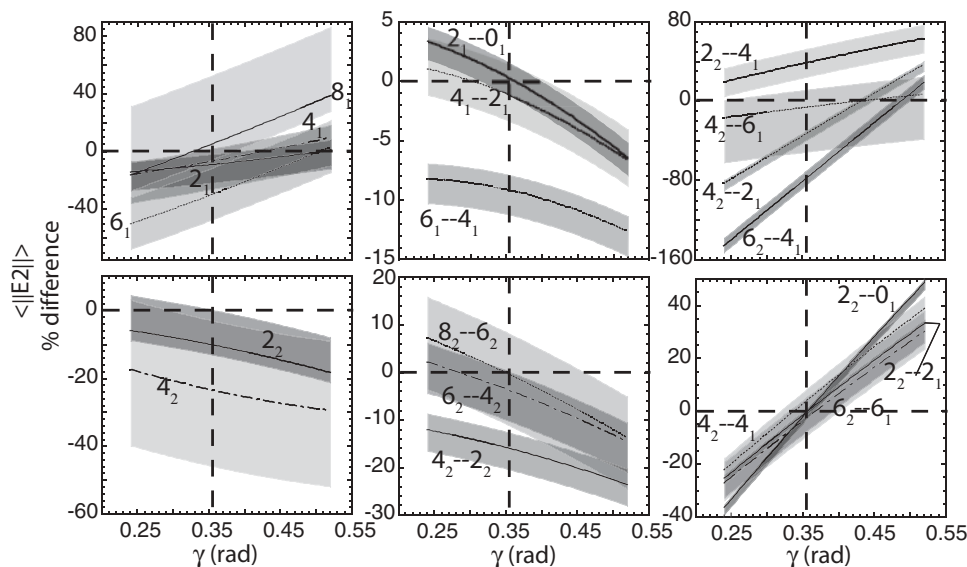

FIG. 3. Differences for calculated vs experimental $E2$ matrix elements for ^{186}Os vs γ. The quantity $\langle \| E2 \| \rangle$ % diff. $= (\langle \| E2 \| \rangle_{th} - \langle \| E2 \| \rangle_{ex}) \times 100 / |\langle \| E2 \| \rangle_{ex}|$. The vertical dashed lines are the "starting" values (cf. Table II) for γ, given here in radians. The shaded zones reflect the uncertainties in the experimental quantities. Quantities labeled, e.g., "4_2" are diagonal matrix elements. (Note the very different vertical scales used.)
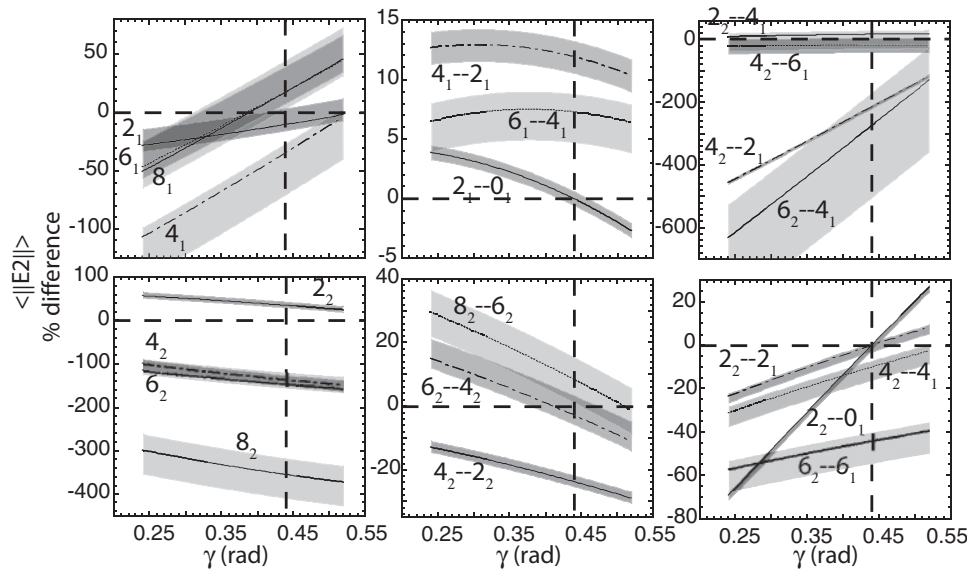
FIG. 4. Same as Fig. 3, but for ^{192}Os.

shown in Fig. 8(b). The values Γ_{irrot} are calculated using [9]

$$\Gamma_{\text{irrot}} = -\frac{1}{2} \cos^{-1} \left(\frac{\cos 4\gamma + 2 \cos 2\gamma}{\sqrt{9 - 8 \sin^2 3\gamma}} \right). \qquad (34)$$

The ratios $\Gamma / \Gamma_{\text{irrot}}$ are 0.441, 0.604, 0.783, and 0.644 for $^{186-192}$Os. The failure of irrotational moments of inertia was noted in Ref. [9]; indeed, the quantities $B(E2; 2_2 \rightarrow 0_1)/B(E2; 2_1 \rightarrow 0_1)$ for $^{186-192}$Os were noted [9] to be the largest known in any nuclei and to lie outside of the physical range for irrotational moments of inertia.

The foregoing comparison of theory with experiment is not a justification for describing these Os isotopes as triaxial, because the description is limited to two-band $\Delta K = 2$ mixing (an identical description would arise if the 2_2^+ states were γ vibrations). To explore the triaxial features exhibited by the Os isotopes requires a comparison between the model and experimental data for the low-lying $K^\pi = 4^+$ bands, cf., Fig. 2. We discuss this below.

The application of a rigid triaxial rotor model to the description of $E2$ properties of the lowest $K^\pi = 4^+$ bands in $^{186-192}$Os requires qualification, because these bands lie, cf. Fig. 2, at $\sim 2\times$ the excitation energy of the lowest $K^\pi = 2^+$ bands, and much lower than the anticipated triaxial $K = 4$ band, which suggests that they have a more nearly harmonic two-phonon vibrational character. However, such an interpretation is a serious over simplification, because detailed spectroscopy reveals significant proton two-quasiparticle character [12] and hexadecapole character [13] (which may be directly related). While this detailed spectroscopic information also rules out a simple rigid rotor model description, the goal of the present calculations for the $K^\pi = 4^+$ bands in these Os isotopes is to explore whether the present model can describe the $K = 4 \rightarrow K = 2$ $E2$ strengths and diagonal matrix elements for those bands.

Burke [16] has extracted the proton two-quasiparticle amplitudes for the $K_{K=4}^+$ states in ^{190,192}Os using a comparison of one-proton transfer strengths into neighboring odd-mass
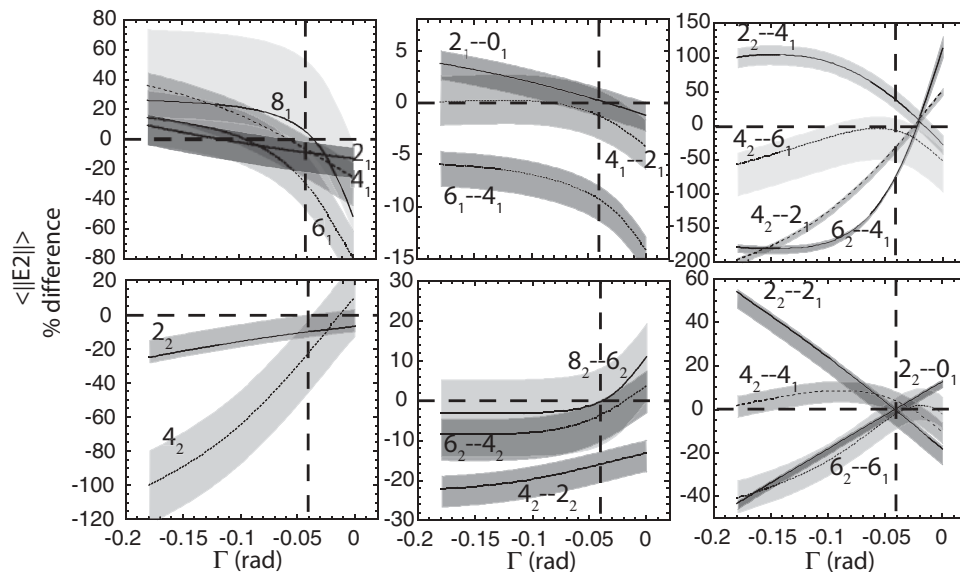
FIG. 5. Differences for calculated vs experimental $E2$ matrix elements for ^{186}Os vs Γ. The quantity $\langle \|E2\| \rangle \%$ diff. $= (\langle \|E2\| \rangle_{\text{th}} - \langle \|E2\| \rangle_{\text{ex}}) \times 100/|\langle \|E2\| \rangle_{\text{ex}}|$. The vertical dashed lines are the "starting" value (cf. Table II) for Γ, given here in radians. See caption to Fig. 3 for further details.
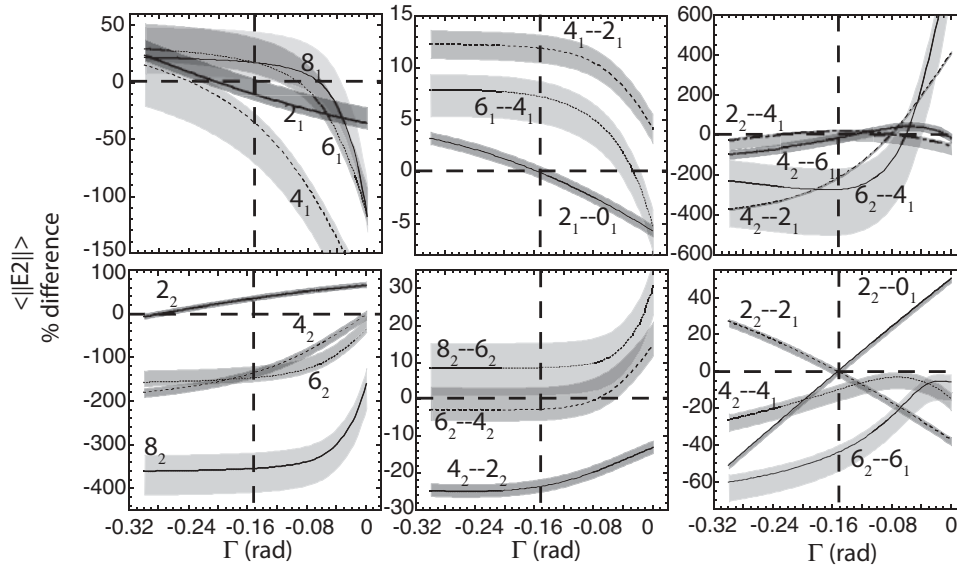
FIG. 6. Same as Fig. 5, but for ^{192}Os.

nuclei. He obtains 0.73 and 0.67, respectively. Burke and coworkers [12] have also tentatively located the other components of the $K_{K=4}^+$ proton two-quasiparticle structure in states at ~2600 keV in ^{190,192}Os. Very recently, similar data have been obtained for ^{186,188}Os [25]. In light of this, we note the following: the most informative comparison is based on the $E2$ trace formula (which is zero, independent of the basis used) for $I = 4$ in the full rotor basis (which possesses three $I = 4$ states), viz.,

$$\text{Tr}\{\hat{T}(E2)\}_{I=4} = Q_0 \cos \gamma \sqrt{\frac{5}{16\pi}} \sqrt{9} \{\langle 40; 20|40 \rangle$$
$$+ \langle 42; 20|42 \rangle + \langle 44; 20|44 \rangle\}, \quad (35)$$

which, from the sum of the Clebsch-Gordan coefficients $(-0.50965, -0.20386, +0.71351)$, is zero. Only the $K = 4$ component gives a positive contribution to the $I = 4$ trace. Therefore, if the experimental "trace" is negative, the implication is that positive $E2$ $(K = 4)$ strength is missing. The missing strengths, according to this sum rule, are given in Table V together with the implied amplitudes of the "non-

model" components of the $K = 4$ states and Burke's [16] and Garrett *et al.*'s [25] deduced amplitudes.

The calculations describing the $\langle \|E2\| \rangle$ values involving the $K^\pi = 4^+$ bands were carried out using diagonalizations in the full model space for each spin up to $I = 6$ and truncated at $K = 6$ for $I = 8$. Two important adjustments were made to the parameters used in the two-band mixing calculations. First, the starting values of Γ were adjusted to the average values obtained from exact fits (cf. Fig. 7) to $2_2 \rightarrow 0_1$ and $4_2 \rightarrow 2_1$. The second is described below.
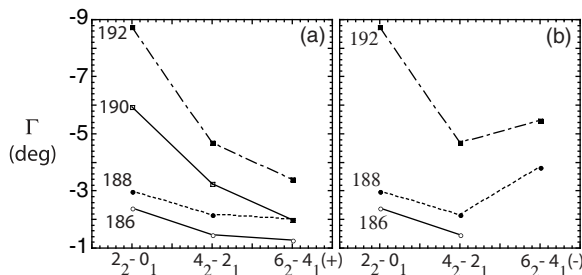

FIG. 7. (a) Exact fit of Γ to the destructively interfering ($\Delta I = -2$ and $\Delta K = -2$) matrix elements (see the discussion in the text). (b) A similar plot to (a) for the choice of negative values for $6_2 - 4_1$, cf. Table I. Thus, there is a model-based preference for positive values for the $6_2 - 4_1$ matrix elements. A negative value for $6_2 - 4_1$ in ^{186}Os cannot be fitted by the model. The positive sign is stated by Wu *et al.* [10] to be better fitted by Coulex data.
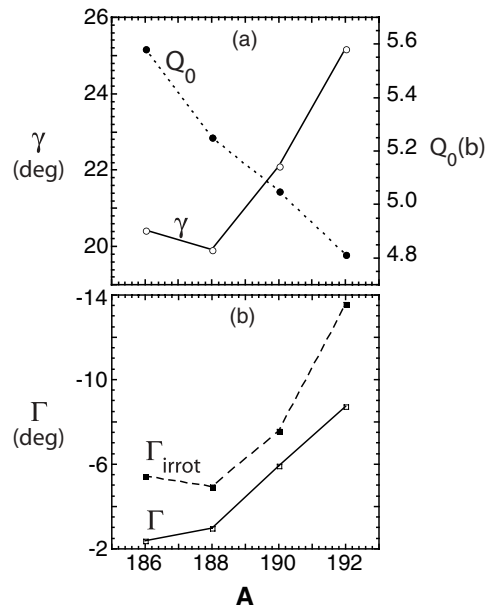

FIG. 8. (a) Systematics of the fitted values of Q_0 and γ, cf. Table II. The anticorrelation is discussed in the text. (b) Systematics of the fitted values of Γ, cf. Table II. The values of Γ_{irrot}, determined using Eq. (34), are also shown.

TABLE V. Experimental $E2$ traces and the deduced "nonmodel" (proton two-quasiparticle) amplitudes of the 4_3^+ states.

	^{186}Os	^{188}Os	^{190}Os	^{192}Os
$\text{Tr}\{\hat{T}(E2)\}_{I=4}$ (eb)	-0.79	-0.54	-1.55	-0.28
$\langle 4_3 \| \hat{T}(E2) \| 4_3 \rangle$ (eb)	2.35	2.68	1.02	1.28
Missing strength[a]	25.2%	16.8%	60.3%	17.9%
Deduced amp[b]	0.502	0.410	0.777	0.424
Garrett/Burke amp	0.45	0.35	0.73	0.67

[a]For ^{186}Os, 2.35 is observed, but $2.35 + 0.79$ is expected.
[b]Deduced amp $= \sqrt{\text{missing strength}/100}$.

The Hamiltonian diagonalized for $I = 4$ was

$$H(4) = \begin{pmatrix} 0 & 12\sqrt{5} & 0 \\ 12\sqrt{5} & 4F/G' & 4\sqrt{7} \\ 0 & 4\sqrt{7} & 16F'/G' \end{pmatrix}, \quad (36)$$

where the common diagonal energy of $20A$ was removed, $F' = 0.38F$ (which lowers the $K = 4$ bands in $^{186-192}$Os to the vicinity of their experimental energies), and the remaining matrix was rescaled by $1/G'$, where G' was obtained from Eq. (6) using the adjusted Γ values, i.e., $G'(\Gamma) = -3.10(-1.95°)$, $-3.04(-2.52°)$, $-4.32(-4.58°)$, and $-5.00(-6.88°)$ for $^{186-192}$Os, respectively, where the G' values are given in keV. The general expression for the off-diagonal matrix elements is [9]

$$\langle IK \pm 2 | H | IK \rangle$$
$$= G\sqrt{(I \mp K)(I \pm K + 1)(I \mp K - 1)(I \pm K + 2)}, \quad (37)$$

or

$$\diamond\langle IK \pm 2 | H | IK \rangle_\diamond$$
$$= G\sqrt{(I \mp K)(I \pm K + 1)(I \mp K - 1)(I \pm K + 2)}$$
$$\times \sqrt{1 + \delta_{K \pm 2, 0}}\sqrt{1 + \delta_{K, 0}}. \quad (38)$$

Thus, the Hamiltonian diagonalized for $I = 6$ was

$$H(6) = \begin{pmatrix} 0 & 4\sqrt{210} & 0 & 0 \\ 4\sqrt{210} & 4F/G' & 6\sqrt{30} & 0 \\ 0 & 6\sqrt{30} & 16F'/G' & 2\sqrt{66} \\ 0 & 0 & 2\sqrt{66} & 36F'/G' \end{pmatrix}. \quad (39)$$

An important point to note here is that the off-diagonal matrix elements decrease with increasing K and, e.g., for ^{192}Os

$$H(6) = \begin{pmatrix} 0 & 57.96 & 0 & 0 \\ 57.96 & -56.62 & 32.86 & 0 \\ 0 & 32.86 & -86.07 & 16.25 \\ 0 & 0 & 16.25 & -193.65 \end{pmatrix}, \quad (40)$$

the off-diagonal element in the $K = 0, 2$ subspace exceeds the difference in the diagonal elements and similarly in the $K = 2, 4$ subspace (but not in the $K = 4, 6$ subspace). For $I = 8$ we truncated at $K = 6$ because, cf. the above remarks, the $K = 8$ mixing does not have a big effect.

The various approximations, described above, are further discussed after presentation of the results.

The results of the full diagonalizations for the $K = 0, 2$ bands are shown in Table VI. Comparing these results with those from the two-band mixing (Table III), we make the following observations:

(i) The $K = 0$ intraband transition matrix elements are virtually unchanged.
(ii) The $K = 2$ intraband transition matrix elements are slightly changed. In particular, the deviations of the $4_2 - 2_2$ matrix elements for $^{186-192}$Os are reduced from -16.0%, -13.1%, -25.2%, and -23.7% to -10.9%, -6.7%, -13.9%, and -4.8%, respectively.
(iii) There are major improvements in the diagonal matrix elements that are poorly fitted in the two-band mixing, e.g., $6_2 - 6_2$ and $8_2 - 8_2$ in ^{190,192}Os.

Evidently, the low values for $6_2 - 6_2$ and $8_2 - 8_2$ observed experimentally are indicative of high-K admixtures. The change in the deviations for $4_2 - 2_2$, $6_2 - 4_2$, and $8_2 - 6_2$ also suggest that high-K admixtures affect the off-diagonal as well as the diagonal γ-band matrix elements. The results for the 4_3^+ states are shown in Table VII and are discussed below.

Table VII reveals that the calculated $E2$ transition strengths from the 4^+, $K = 4$ states to the 2^+, 3^+, 4^+, $K = 2$ states are generally smaller than the experimental values, which suggests that the $K^\pi = 4^+$ structure has enhanced $\Delta K = 2$, $E2$ strength, e.g., from a larger value of γ. The calculated diagonal matrix elements for the 4^+, $K = 4$ states are uniformly larger than the experimental values. This is a model quantification of the sum rule implicit in Eq. (35) and is discussed in the foregoing text. (We note that the model value for the $4_3 - 3_1$ matrix element, cf. footnote to Table I, is positive; Wu *et al.* [10] assumed it to be negative.)

The approximations made in the present study need qualification. The primary aim of this study has been to explore how well the triaxial rotor model can describe doubly even nuclei, in particular, nuclei that possess excited states which suggest that they may be triaxial and for which there is a large set of $E2$ matrix elements. The isotopes $^{186-192}$Os are the best choice for this exercise, but the lowest $K = 4$ bands in these isotopes do not have a simple structure. From the $K = 0, 2$ two-band mixing approximation, the results indicate a serious failing in the description of the diagonal matrix elements which are observed to be much smaller. Mixing of the low-lying high-K bands explains this. To effect this mixing, we used some very simple approximations with the aim of clarifying what was behind the calculation. To carry out a more realistic calculation, a second $K = 4$ band is certainly needed, but this would involve many more parameters. The magnitudes of the off-diagonal vs the diagonal matrix elements also would need to be explored. In the form employed, viz., F/G', F'/G', there is the issue of the modification of both G (cf. Fig. 7) and F. The spin dependence of the parameters in the Hamiltonian [cf. Eq. (1)] is well known for A (cf. the energies of the ground-state bands in Fig. 2) and has been pointed out in this study for G, but this will also be likely for F.

During the course of this work, a version of the Bohr Hamiltonian with γ-soft and triaxial rotor degrees of freedom was applied to the osmium isotopes by Fortunato and coworkers [26]. The focus of their work was on excitation energies and the observation of the $K = 4$ bands well below the rigid triaxial rotor energy. Their work did not consider the extensive

TABLE VI. Values of $\langle\|E2\|\rangle$ in eb calculated using the full diagonalization as described in the text for $^{186-192}$Os. The values of F and G used differ from Table II and are discussed in the text. See the caption to Table III for the explanation of other details.

	^{186}Os	^{188}Os	^{190}Os	^{192}Os
$2_1 - 0_1$	1.6697 (−0.3%)	1.5812 (−0.2%)	1.5190 (−0.7%)	1.4414 (−1.0%)
$4_1 - 2_1$	2.7170 (−1.6%)	2.5761 (−2.5%)	2.4853 (+5.0%)	2.3628 (+11.7%)
$6_1 - 4_1$	3.512 (−9.7%)	3.338 (+0.8%)	3.2369 (+9.0%)	3.1448 (+7.3%)
$8_1 - 6_1$	4.237 (−1.9%)	4.035 (+1.6%)	4.009 (+7.8%)	3.840 (+7.3%)
$4_2 - 2_2$	1.7509 (−10.9%)	1.661 (−6.7%)	1.6115 (−13.9%)	1.5580 (−4.8%)
$6_2 - 4_2$	2.865 (+3.0%)	2.668 (+8.5%)	2.224 (−14.5%)	2.172 (+3.9%)
$8_2 - 6_2$	3.550 (+8.9%)	3.303 (+29.5%)	3.105 (+19.4%)	2.906 (+25.8%)
$2_2 - 0_1$	0.5581 (+2.4%)	0.4958 (+2.6%)	0.4800 (+8.1%)	0.4771 (11.0%)
$2_2 - 2_1$	0.8668 (−3.4%)	0.8362 (−3.3%)	0.9888 (−7.2%)	1.1406 (−7.3)
$2_2 - 4_1$	0.2949 (+29.9%)	0.3072 (−18.7%)	0.401 (+111.0%)	0.455 (+30.0%)
$4_2 - 2_1$	0.3471 (−17.2%)	0.2357 (−16.7%)	0.0572,(−71.8%)	−0.0402 (−130.9%)
$4_2 - 4_1$	1.2524 (+2.7%)	1.187 (+7.9%)	1.2849 (−10.5%)	1.309 (−3.1%)
$4_2 - 6_1$	0.634 (−5.4%)	0.640 (+12.2%)	0.867 (+31.3%)	0.587 (+46.8%)
$6_2 - 4_1$	0.1535 (−52.8%)	0.0141 (−88.9%)	−0.3927 (−301.4%)	−0.1797 (−360.4%)
$6_2 - 6_1$	1.406 (+2.6%)	1.276 (−12.6%)	1.123 (−36.2%)	1.105 (−25.9%)
$2_1 - 2_1$	−1.917 (−9.6%)	−1.795 (−3.8%)	−1.627 (−30.2%)	−1.411 (−16.7%)
$4_1 - 4_1$	−2.218 (−9.8%)	−2.017 (−0.8%)	−1.576 (−23.1%)	−1.104 (−51.3%)
$6_1 - 6_1$	−2.261 (−35.40%)	−1.987 (−24.2%)	−1.170 (−28.6%)	−0.822 (+29.2%)
$8_1 - 8_1$	−2.160 (+4.4%)	−1.874 (−35.8%)	−1.234 (−31.3%)	−0.719 (+45.1%)
$2_2 - 2_2$	1.917 (−9.6%)	1.795 (−14.5%)	1.627 (+6.3%)	1.4115 (+43.3%)
$4_2 - 4_2$	−1.179 (−5.3%)	−1.136 (+6.9%)	−1.102 (+15.6%)	−0.826 (+0.5%)
$6_2 - 6_2$	−2.168 (⊘)	−1.938 (−45.7%)	−0.818 (−2.2%)	−0.751 (+44.4%)
$8_2 - 8_2$	−2.547 (⊘)	−2.181 (⊘)	−1.484 (−41.3%)	−0.999 (−9.7%)

set of $E2$ matrix elements available from the multi-Coulex study of Wu *et al.* [10], and so it is not possible to compare their calculations with ours. Also, that work did not consider the evidence for hexadecapole and proton two-quasiparticle character in the 4^+, $K = 4$ states, which has been a leading concern in our study.

In summary, the triaxial rotor model with independent inertia and $E2$ tensors [9] is able to provide a uniform quantitative description of large sets of $E2$ matrix elements in candidate triaxial nuclei. The apparently counter-intuitive feature of decreasing diagonal matrix elements and increasing transition matrix elements, with increasing spin, involving the same sets of states is explained as being due to admixtures of higher K band configurations into the low K bands. The electric quadrupole parameter Q_0 remains stable with increasing spin, as reflected in the description of transition matrix elements in the ground-state band. The separation of triaxiality of the electric quadrupole tensor from the triaxiality of the inertia tensor (the angles γ and Γ) in the model shows that there is a dependence of Γ on spin (Fig. 7) such that, cf. Eq. (6), G decreases with increasing spin. We note that this would explain nonlinearities in Mikhailov plots, such as were observed in our precision study [27] of ^{166}Er, i.e., a decreasing magnitude of the slope, M_2, at high spin (cf. Fig. 5 in Ref. [27]). Indeed, the energy parameters A and G of the model exhibit a spin dependence. This is widely known for A, but is revealed here to be true also for G. The implication is that F is also spin dependent. The description of the $E2$ properties of the 4^+, $K = 4$ state strongly points to missing $E2$ strength in the Os isotopes. This agrees with

TABLE VII. Values of $\langle\|E2\|\rangle$ in eb involving the $4_3^+(K = 4)$ states calculated using the full diagonalization as described in the text and the caption to Table VI.

	^{186}Os	^{188}Os	^{190}Os	^{192}Os
$4_3 - 2_1$	∼0.000(−100.4%)	0.0058 (−95.2%)	0.0395 (−24.1%)	0.0916 (−20.4%)
$4_3 - 2_2$	0.7971 (−33.0%)	0.677 (−18.4)	0.554 (−28.1%)	0.4206 (−46.5%)
$4_3 - 3_1$	0.975 (−35.8%)	0.970 (−17.1%)	1.217 (−21.5%)	1.433 (−12.1%)
$4_3 - 4_2$	0.899 (−50.8%)	0.975 (−40.5%)	1.468 (−7.6%)	1.960 (+64.7%)
$4_3 - 4_3$	3.397 (+44.5%)	3.153 (+17.7%)	2.678 (+162.6%)	1.930 (+50.8)

Burke's one-proton transfer reaction studies of these states in ^{190,192}Os and very recent similar studies in ^{186,188}Os [25]. This is of more than "local" interest, because Burke [18] noted that similar complex behavior of $K^{\pi} = 4^+$ structures is occurring at $N = 90$. This was recently confirmed in ^{152}Sm by Kulp and Garrett [28]. It is possible that our understanding of low-lying collective 4^+, $K = 4$ states is very inadequate.

In conclusion, the present study reveals some clear strengths in support of a triaxial rotor description of $^{186-192}$Os and some clear weaknesses. The strengths are outlined in the previous paragraph. The weaknesses reside in a number of ambiguities that involve the $K^{\pi} = 4^+$ excited bands in these nuclei. These bands, if they are the only collective $K^{\pi} = 4^+$ bands in $^{186-192}$Os, are too low in energy to be pure triaxial rotor bands. The success of this model with respect to the $K = 0$ and $K = 2$ bands is insufficient to necessitate the triaxial features of the model: as pointed out, the model would only be a way of doing two-band mixing with no insight into the intrinsic structure of the $K = 2$ band (e.g., it could be a γ vibration). However, this study reveals, through the trace relationship of Eq. (35), that

there is missing $E2$ diagonal strength [11] and that there must be (at least) a second $K = 4$ band which carries the missing strength. Data from one-proton transfer reactions [12,25] and inelastic scattering [13] also demand (at least) a second $K = 4$ band. To further clarify this ambiguity, this band needs to be found in $^{186-192}$Os. In addition, to provide a test of the present model, the interband $E2$ transition strengths between this second $K = 4$ band and the $K = 2$ band and the interband and intraband $E2$ strength for this second and the first $K = 4$ band will be needed. Before such information is obtained, the issue of γ deformation vs γ softness (or some combination of the two) in $^{186-192}$Os cannot be answered.

[1] A. S. Davydov and G. F. Filippov, Nucl. Phys. **8**, 237 (1958).

[2] A. S. Davydov, At. Energy Rev. **6**, 3 (1968).

[3] A. Bohr and B. R. Mottelson, *Nuclear Structure*, Vol. II (Benjamin, Reading, MA, 1975).

[4] S. Frauendorf, Rev. Mod. Phys. **73**, 463 (2001); I. Hamamoto, Phys. Rev. C **65**, 044305 (2002).

[5] J. B. Gupta and S. Sharma, Phys. Scr. **39**, 50 (1989); H. M. Mittal, S. Sharma, and J. B. Gupta, *ibid.* **43**, 558 (1991).

[6] J. Yan, O. Vogel, P. Von Brentano, and A. Gelberg, Phys. Rev. C **48**, 1046 (1993).

[7] C. Y. Wu and D. Cline, Phys. Rev. C **54**, 2356 (1996).

[8] L. Esser, U. Neuneyer, R. F. Casten, and P. Von Brentano, Phys. Rev. C **55**, 206 (1997).

[9] J. L. Wood, A. M. Oros-Peusquens, R. Zaballa, J. M. Allmond, and W. D. Kulp, Phys. Rev. C **70**, 024308 (2004); J. M. Allmond, Ph.D. dissertation, Georgia Institute of Technology (2007), http://hdl.handle.net/1853/14604.

[10] C. Y. Wu, D. Cline, T. Czosnyka, A. Backlin, C. Baktash, R. M. Diamond, G. D. Dracoulis, L. Hasselgren, H. Kluge *et al.*, Nucl. Phys. **A607**, 178 (1996).

[11] C. Y. Wu *et al.*, Phys. Rev. C **64**, 014307 (2001).

[12] R. D. Bagnell, Y. Tanaka, R. K. Sheline, D. G. Burke, and J. D. Sherman, Phys. Rev. C **20**, 42 (1979).

[13] F. T. Baker, A. Sethi, V. Penumetcha, G. T. Emery, W. P. Jones, M. A. Grimm, and M. L. Whiten, Nucl. Phys. **A501**, 546 (1989); F. T. Baker, T. H. Kruse, W. Hartwig, I. Y. Lee, and J. X. Saladin, *ibid.* **A258**, 43 (1976).

[14] D. G. Burke, Phys. Rev. C **66**, 039801 (2002).

[15] C. Y. Wu *et al.*, Phys. Rev. C **66**, 039802 (2002).

[16] D. G. Burke, Phys. Lett. **B406**, 200 (1997).

[17] C. Y. Wu and D. Cline, Phys. Lett. **B382**, 214 (1996).

[18] D. G. Burke, Phys. Rev. Lett. **73**, 1899 (1994).

[19] C. M. Baglin, Nucl. Data Sheets **99**, 57 (2003).

[20] B. Singh, Nucl. Data Sheets **95**, 413 (2002).

[21] B. Singh, Nucl. Data Sheets **99**, 285 (2003).

[22] C. M. Baglin, Nucl. Data Sheets **84**, 723 (1998).

[23] M. V. Hoehn, E. B. Shera, H. D. Wohlfahrt, Y. Yamazaki, R. M. Steffen, and R. K. Sheline, Phys. Rev. C **24**, 1667 (1981).

[24] W. Andrejtscheff and P. Petkov, Phys. Rev. C **48**, 2531 (1993).

[25] P. E. Garrett, A. A. Phillips, L. Bettermann, N. Braunn, D. G. Burke *et al.* in conference proceedings (unpublished).

[26] L. Fortunato, S. De Baerdemacker, and K. Heyde, Phys. Rev. C **74**, 014310 (2006).

[27] W. D. Kulp, J. M. Allmond, P. Hatcher, and J. L. Wood *et al.*, Phys. Rev. C **73**, 014308 (2006).

[28] W. D. Kulp and P. E. Garrett (private communication).